

Effects of Resonant Magnetic Perturbation on Particle Transport in LHD^{*)}

Kenji TANAKA, Marcin JAKUBOWSKI¹⁾, Andreas DINKLAGE¹⁾, Yasuhiro SUZUKI, Motoshi GOTO, Tomohiro MORISAKI, Satoru SAKAKIBARA, Yoshiro NARUSHIMA, Tsuyoshi AKIYAMA, Tokihiko TOKUZAWA, Kazuo KAWAHATA, Ryo YASUHARA, Ichihiko YAMADA, Suguru MASUZAKI, Mikirou YOSHINUMA, Katsumi IDA, Leonid VYACHESLAVOV²⁾, Clive MICHAEL³⁾, David MIKKELSEN⁴⁾ and Todd EVANS⁵⁾

National Institute for Fusion Science, Toki 509-5292, Japan

¹⁾*Max-Planck Institut für Plasmaphysik, Greifswald, Germany*

²⁾*Budker Institute of Nuclear Physics, SB RAS, Novosibirsk, Russia*

³⁾*Australian National University, Canberra, Australia*

⁴⁾*Princeton Plasma Physics Laboratory, New Jersey, U.S.A.*

⁵⁾*General Atomics, San Diego, California, U.S.A.*

(Received 7 December 2012 / Accepted 12 July 2013)

In this study, the effects of resonant magnetic perturbation (RMP) on particle transport are investigated in Large Helical device (LHD). The magnetic configuration is selected to be the outwardly shifted configuration, for which the magnetic axis position (R_{ax}) is 3.9 m. At $R_{ax} = 3.9$ m, the main plasma is surrounded by a thick ergodic layer, with width of about 30% of the plasma minor radius. The perturbation mode $m/n = 1/1$, where m and n are poloidal and toroidal mode numbers, is applied. The resonant layer is around the last closed flux surface. With RMP, a region in which both the connection and Kolmogorov lengths are finite and the magnetic field is ergodic forms; this region extends inside the main plasma. In the low-collisionality regime, where $\nu_h^* < 1$ ($\nu_h^* = 1$ is the boundary between the $1/\nu$ and plateau regimes in stellarator/helical neoclassical transport), there is no apparent difference in particle transport with and without RMP. However, in the high-collisionality regime ($\nu_h^* > 1$), a clear difference in particle transport is found. A clear difference in turbulence is also observed, suggesting that turbulence plays a significant role in particle transport in the high-collisionality regime both with and without RMP.

© 2013 The Japan Society of Plasma Science and Nuclear Fusion Research

Keywords: LHD, resonant magnetic perturbation, particle transport, turbulence, phase contrast imaging

DOI: 10.1585/pfr.8.2402141

1. Introduction

Resonant magnetic perturbation (RMP) coils are one of the most effective control tools for mitigating edge localized mode (ELM) activity in tokamaks [1]. In addition to ELM mitigation, RMP also affects transport. For example, in DIII-D, enhancement of particle transport, the so-called particle pump-out, has been reported [1]. Understanding the effects of RMPs on transport is essential for ELM mitigated operations in tokamaks. In contrast to tokamaks, 3D devices allow detailed assessments of the effects of stochastic fields on transport. In LHD, ELM-like events have been observed in H modes at relatively high plasma β [2]. Although ELMs are not, at present, regarded as a critical issue for the LHD, the effects of RMPs on transport can be used as a tool to control transport.

The experiments reported in this paper were con-

ducted using the outwardly shifted configuration, with the magnetic axis position at 3.9 m; the width of the ergodic layer was about 30% of the plasma minor radius.

2. Magnetic Topology

Figure 1 compares Poincaré plots with and without RMP, as calculated by an HINT2 code [3]. Magnetic perturbation induces an $m/n = 1/1$ island around the last closed flux surface (LCFS). The safety factor at LCFS is close to one. The calculations were performed assuming magnetic equilibrium and a linear superposition of external perturbations.

As shown in Fig. 1, the main plasma is surrounded by a thick ergodic layer. Figure 1 (a) shows that, without RMP, some islands exist naturally, such as $m/n = 20/22$ and $10/10$. With RMP, the $m/n = 1/1$ island is not clearly observed in Fig. 1 (b). This is because the ergodic region is more stochastic, which results in larger island overlaps from higher order modes. This is in clear contrast to the

author's e-mail: ktanaka@nifs.ac.jp

^{*)} This article is based on the presentation at the 22nd International Toki Conference (ITC22).

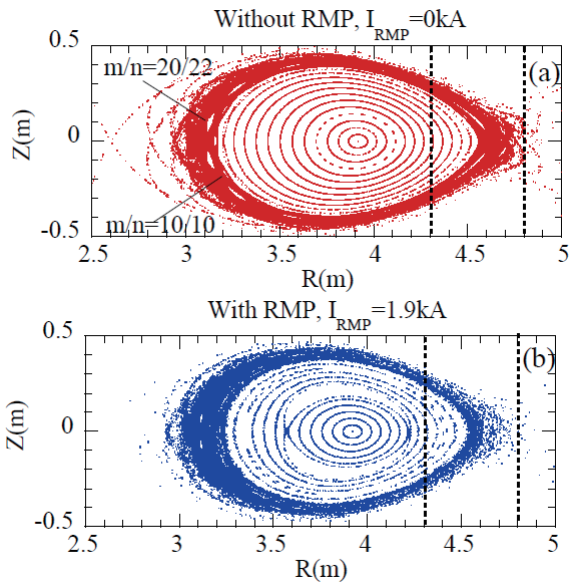


Fig. 1 Poincaré plots of plasma (a) without RMP and (b) with RMP.

configuration at $R_{ax} = 3.6$ m, where the $m/n = 1/1$ island is inside LCFS and a nested surface exists outside the island separatrix [4]. The interaction between RMP and the existing equilibrium field modifies the magnetic topology. However, with RMP, the $m/n = 2/1$ island is clearly observed around $\rho = 0.5$.

Figure 2 shows spatial profiles of connection length (L_c), Kolmogorov length (L_k), and rotational transform (ι), which is the inverse of the safety factor. These quantities were calculated at $Z = 0$ m and within the range $R = 4.3 - 4.8$ m, which is indicated by dashed lines in Fig. 1. The connection length is the distance of the magnetic field from the calculation starting point to the closest intersection point with plasma facing components. The calculation of L_c was stopped when it reached 1 km. Positions at which L_c is greater than 1 km roughly correspond to vacuum-nested flux surfaces. As shown in Fig. 2 (a), L_c becomes 1 km at $R < 4.62$ m without RMP and at $R < 4.58$ m with RMP.

The Kolmogorov length is a measure of the exponential separation of field lines. It is a good indicator of whether a magnetic field line is stochastic. Figure 2 (b) shows that the Kolmogorov length in the finite L_c region becomes slightly shorter with RMP.

3. Experimental Results

Figure 3 compares time traces with and without RMP. The plasma heating conditions were identical for the two cases. After plasma production by a 77-GHz ECRH, two tangentially injected negative-ion-based neutral beams (N-NB) were injected in series. The power was initially 5.5 MW. Then, beginning at $t = 5.3$ s, the N-NB was reduced to 2 MW. Both N-NB beams were injected in the

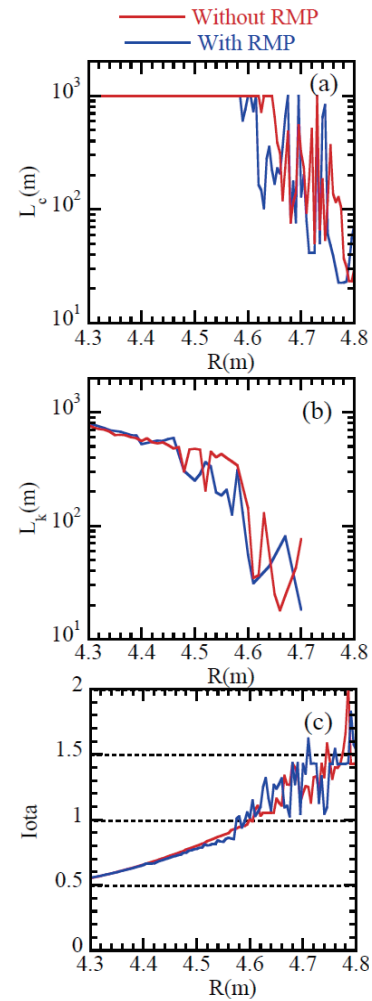


Fig. 2 Effects of RMP on (a) connection length, (b) Kolmogorov length, and (c) rotational transform $\iota (= 1/q)$. The region between the two dashed lines at $Z = 0$ m in Fig. 1 are shown here.

co-toroidal field direction. By changing the injected beam power, we realized two phases with different plasma collisionalities: (a) during 3.8 - 5.2 s, the plasma was in a low-collisionality phase because of low density and high temperature, and (b) after 5.4 s, the plasma was in a high-collisionality phase because of high density and low temperature. These two phases are used to explain the experimental observations and analysis results. To produce a density modulation, external fueling was modulated at 5 Hz; this was done to estimate diffusion coefficients (D) and convection velocities (V) [5]. As shown in Fig. 3 (a), in the low-collisionality phase, the density was clearly modulated with and without RMP. However, in the high-collisionality phase, the density was modulated with RMP but not without RMP. External fueling is a feedback control through which we try to maintain constant density; thus, fueling was reduced after reduction in heating power at $t = 5.3$ s. This is due to better particle confinement with lower heating power. In other words, better confinement is attained during the high-collisionality phase [5]. Exter-

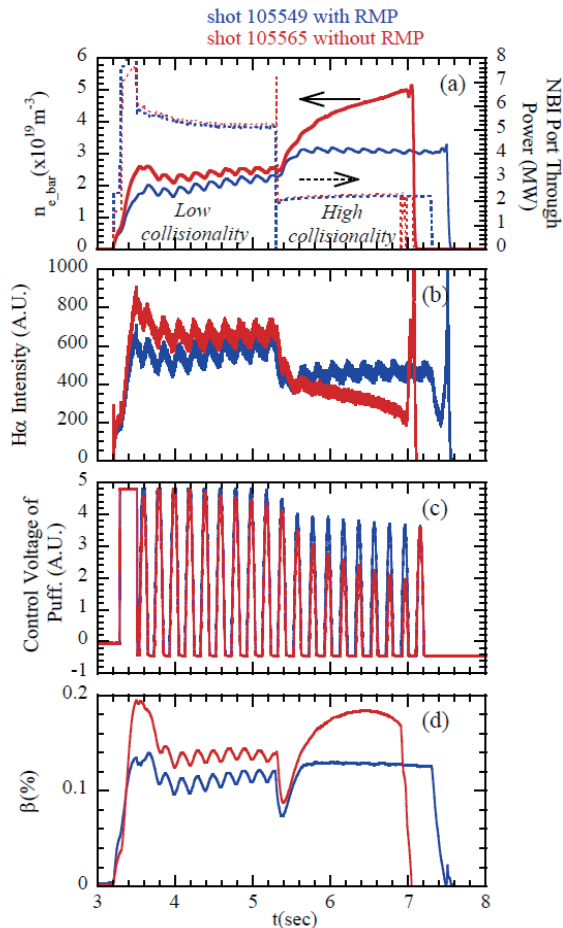


Fig. 3 Effects of RMP on time traces for (a) line averaged density, (b) $H\alpha$, (c) gas fueling control signal, and (d) volume averaged β , $R_{ax} = 3.9$ m, $B_t = 2.54$ T.

nal fueling was smaller after $t = 5.3$ s without RMP. The tendency for particle confinement to improve in the high-collisionality regime was stronger without RMP. Note that this difference was caused by applying RMP. The results indicate that RMP can be employed as an actuator for particle transport in the high-collisionality regime.

3.1 Effects of RMP on profiles

Figure 4 compares profiles in the low-collisionality phase with and without RMP. The electron density and temperature profiles were obtained by Thomson scattering [6]. Turbulences were measured by two-dimensional phase contrast imaging (2D-PCI) [7]. 2D-PCI measures poloidally dominated wavenumber components of ion scale turbulence ($k\rho_i = 0.1 - 1$, where ρ_i is the ion Larmor radius). Since 2D-PCI measures turbulence at a different cross section, the profiles are shown in flux surface coordinates. The turbulence position was determined from the propagation direction, which was perpendicular to the local magnetic field, and from equilibrium data [7].

As shown in Figs. 4(a-1) and 4(a-2), the density was slightly higher without RMP. This was likely due to differ-

ence of fueling, which is indicated by the $H\alpha$ intensity and gas valve control waveforms, as shown in Figs. 3(b) and 3(c). The shapes of n_e and T_e profiles are almost identical, and the turbulence profiles are not very different. A turbulence peak exists around $\rho = 1$, and the dominant components propagate in the electron diamagnetic direction in the laboratory frame. Small turbulence components exist around $\rho = 1.2$, which propagate toward the ion diamagnetic direction in the laboratory frame. Assuming the turbulence phase velocity was dominated by $E_r \times B_t$ poloidal rotation velocity, these observations indicate a negative E_r around $\rho = 1$ and a positive E_r around $\rho = 1.2$. Note that, in the low-collisionality phase, the profiles exhibit almost no differences with and without RMP. Also, no T_e and n_e flattening is observed at the $m/n = 2/1$ island around $\rho = 0.5$ or at the $m/n = 1/1$ island around $\rho = 1.0$. This indicates that these islands are healed in the low-collisionality phase.

Figure 5 compares profiles with and without RMP in the high-collisionality phase. In contrast to Figs. 4(a-1) and 4(b-1), flattening of n_e and T_e appears in the profiles around $\rho = 1$ as shown in Figs. 5(a-1) and (b-1), which corresponds to the location of the $m/n = 1/1$ island with RMP. However, no flattening is observed at the $m/n = 2/1$ island around $\rho = 0.5$. The $m/n = 2/1$ island is healed, but the $m/n = 1/1$ island appeared.

In a previous study, the healing condition of the $m/n = 1/1$ island has been well-clarified [4]. The island is healed with increasing β and decreasing collisionality. As shown in Fig. 3(a), the volume-averaged β with RMP is almost constant in the low-collisionality phase ($t = 4 - 5.2$ s) and in the high collisionality phase ($t = 5.6 - 7.4$ s). After reduction in heating power, density increases and temperature decreases, as shown in Figs. 4(a-1) and 4(b-1) and Figs. 5(a-1) and 5(b-1), so β remains almost constant while collisionality increases. The observation of island healing in the low-collisionality phase ($t = 4 - 5.2$ s) with RMP is consistent with previous results [4]. The phase velocity is higher toward the electron diamagnetic direction in the low-collisionality phase (Fig. 4(e-1)) than in the high-collisionality phase (Fig. 5(e-1)). This qualitatively agrees with recent results in which the increase in $E_r \times B_t$ rotation velocity toward the electron diamagnetic direction heals the $m/n = 1/1$ island [8]. One theoretical explanation for this island healing is the balance of electromagnetic torque due to the magnetic island and neoclassical flow damping [9].

In the high-collisionality phase, n_e , T_e , and turbulence profiles are clearly different with and without RMP, as shown in Fig. 5. Without RMP, the turbulence peak is more inward and the phase velocity at the turbulence peak is smaller than that with RMP.

Figure 6 compares profiles in the edge region with and without RMP. Full profiles are shown along the R -axis at $Z = 0$ (Fig. 1) to compare the findings with magnetic properties, as shown in Fig. 2. For the same reason, the turbulence

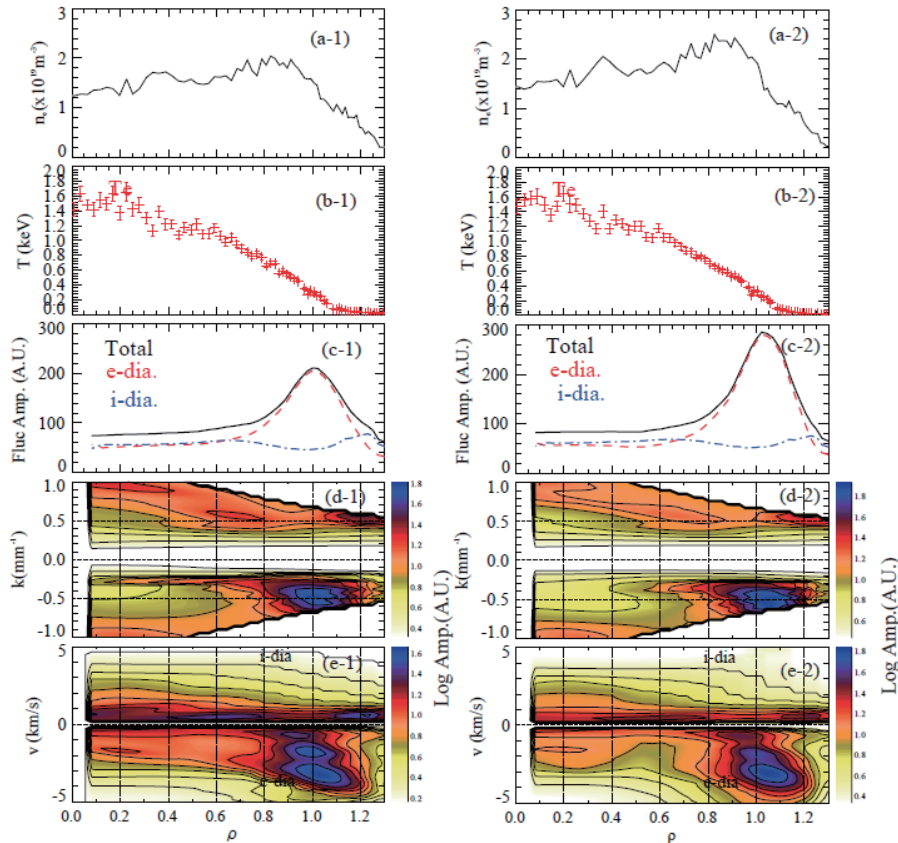


Fig. 4 Low-collisionality phase of (a) n_e , (b) T_e at $t = 4.55$ s, (c) turbulence amplitude, (d) k spectrum, and (e) turbulence phase velocity at $t = 4.5 - 4.7$ s. (a-1) - (e-1) with RMP, shot 105549, (a-2) - (e-2) and without RMP, shot 105565.

profiles are also mapped on R .

Spatial profiles of ionization rate are shown in Figs. 6 (b) and 6 (e). The spatial profile of ionization rate is determined from the cross section of ionization and Doppler broadening of $H\alpha$ intensity [10, 11]. The decomposition of a broadened spectrum can determine the spatial position of $H\alpha$ radiation because broadening is a function of the local T_e . For this calculation, T_e was assumed to be equal to T_i . Absolute calibration was not well-done, but, from these figures, the shapes of the ionization rates can be seen and a relative comparison is possible. Using this technique, the uncertainty in ionization due to the local T_e is around 20% at $T_e = 10 - 30$ eV. This corresponds to the region for which $R > 4.7$ m. This effect is negligible at $T_e > 30$ eV for $R < 4.7$ m; however, there are other uncertainties. The ruling factor is the finite mean free path for ionization, which is around 3 cm for $R = 4.3 - 4.7$ m. These effects do not influence the conclusions drawn here. Uncertainties in the determination of ionization profiles are described in detail in [10].

As shown in Fig. 6 (b), the n_e profile and ionization rate do not change clearly in the low-collisionality phase with and without RMP. This suggests that particle transport also does not differ. In other words, RMP does not affect particle transport characteristics in the low-collision phase.

However, the n_e profile is clearly different in the high-

collisionality phase with and without RMP, as shown in Fig. 6 (e). At $R > 4.7$ m, the ionization rate is a factor of 2-5 higher with RMP, but the density is only around 10% higher with RMP. At $R < 4.65$ m, the ionization rate is slightly higher (factor of 1-2) with RMP, but the density is 30% - 50% lower. These provide clear evidence that RMP enhances particle transport.

In Fig. 6, the peak positions of the turbulence amplitude are indicated by dashed lines. In the low-collisionality phase, the peak position is almost the same with and without RMP. In the high-collisionality phase, the peak position with RMP at 4.58 m correlates with the radial location of the $m/n = 1/1$ island (Figs. 1 and 2). With RMP, the peak position of turbulence moves to the inner side; without RMP, the turbulence peak clearly exists at a flat density gradient regime. In contrast, with RMP, it is not clear whether the turbulence peak exists in the flat density gradient region inside the island or in the steep density gradient region at the boundary of the island. If the latter is the case, the difference in density gradients at the turbulence peaks may characterize the different natures of turbulence.

Gyrokinetic linear analysis shows that positive density gradients drive the trapped electron mode (TEM) and that negative density gradients drive the ion temperature gradient mode (ITG) close to $\rho = 1$ [12]. Thus, these differences in turbulence nature may be linked to those in par-

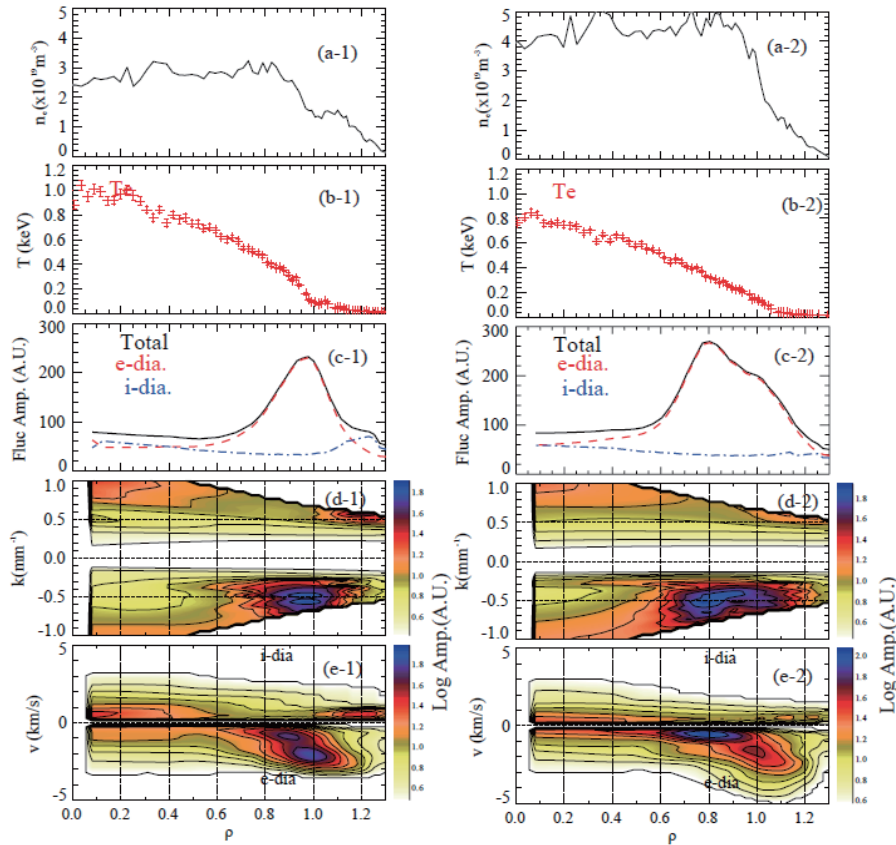


Fig. 5 High-collisionality phase of (a) n_e , (b) T_e , at $t = 6.55$ s, (c) turbulence amplitude, (d) k spectrum, and (e) turbulence phase velocity at $t = 6.5 - 6.7$ s. (a-1) - (e-1) with RMP, shot 105549 (a-2) - (e-2) and without RMP, shot 105565.

ticle transport with and without RMP.

3.2 Effects of RMP on particle transport

To obtain more quantitative information on particle transport characteristics, two analysis techniques were applied: density modulation [5] and the estimation of local particle confinement time using ionization rate profiles [10, 11]. Using the former, it is possible to separately estimate diffusion coefficients (D) and convection velocities (V). The results are independent of the ionization rate's absolute value. However, as shown in Fig. 3, since density is not always modulated in the high-collisionality phase, the latter technique is used to analyze RMP effects on particle transport in the high-collisionality phase.

The particle balance equation is written here as

$$\frac{\partial n_e}{\partial t} = -\nabla \cdot \Gamma + S = -\frac{1}{r} \frac{\partial}{\partial r} r\Gamma + S, \quad (1)$$

where S is the ionization rate and Γ is the particle flux.

$$\Gamma = -D\nabla n_e + n_e V. \quad (2)$$

The modulation amplitude \tilde{n}_e of the particle balance equation is given by

$$\begin{aligned} \frac{\partial^2 \tilde{n}_e}{\partial r^2} + \left(\frac{1}{r} + \frac{1}{D} \frac{\partial D}{\partial r} - \frac{V}{D} \right) \frac{\partial \tilde{n}_e}{\partial r} - \left(\frac{V}{rD} + \frac{1}{D} \frac{\partial V}{\partial r} \right) \tilde{n}_e \\ - i \frac{\omega}{D} \tilde{n}_e + \frac{\tilde{S}}{D} = 0. \end{aligned} \quad (3)$$

In (3), ω is the modulation frequency and \tilde{S} is the modulated component of the ionization rate. Equation (3) consists of two sets of equations: the real and imaginary parts of the modulation components. Figure 7 shows the models used for D and V . Values for D and V were determined from a fitting procedure that matches the solution of (3) to experimental data. For a stable fit, both real and imaginary modulation components, which correspond to the modulation amplitude and phase, and the equilibrium profiles were fit simultaneously [5].

For the analysis of modulation experiments, interferometer data were used and the density was assumed to be constant on flux surfaces. This is possible inside the last closed flux surface. Outside of LCFS, nested isodensity surfaces were assumed for extrapolation. The existence of the $m/n = 1/1$ island may affect the estimation of D and V ; however, this effect is considered to be small since the estimated D and V are spatially averaged values in the core over $\rho = 0.4 - 0.7$ and in the edge over $\rho = 0.7 - 1.0$, while the island width is around $\Delta\rho = 0.1$ at $\rho = 1$.

When D is small or V is strongly outward, the modulation amplitude is localized in the edge, and the analysis becomes insensitive to core diffusion. Thus, the model of spatially constant D was used, as shown in Fig. 7 (a). When D is large or V is small or is large and pointing inward, the modulation penetrates deeply into the core. Thus, the two-

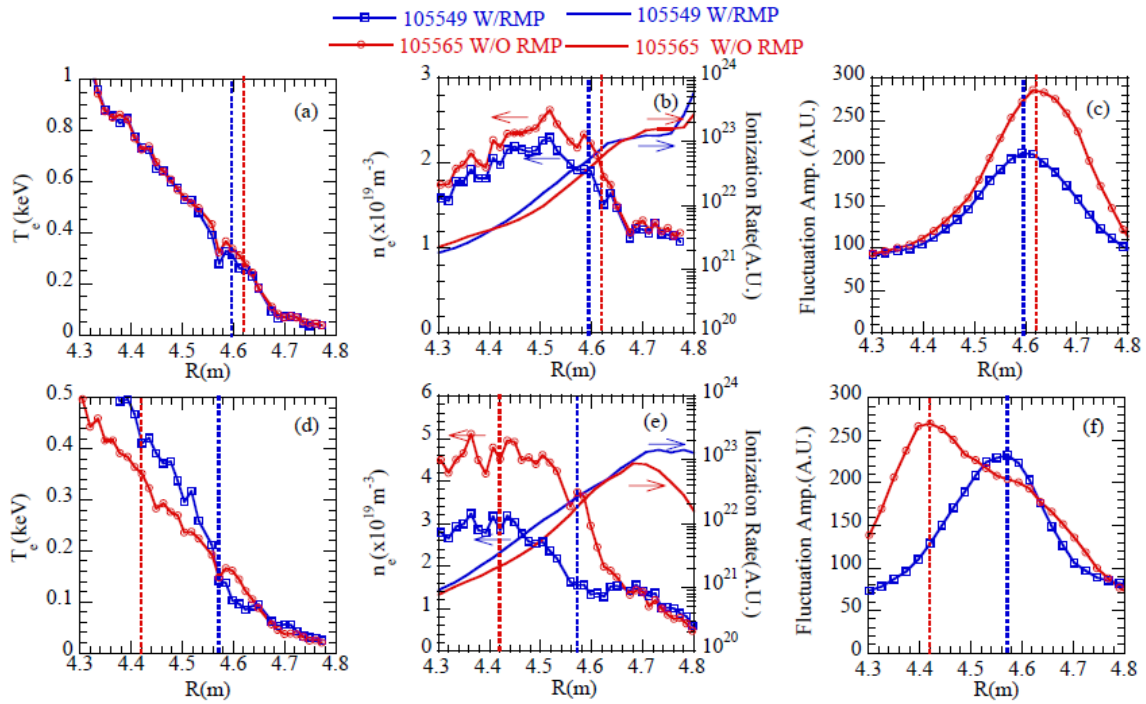


Fig. 6 Expanded views of edge region (a) and (d) T_e , (b) and (e) n_e and ionization rate, (c) and (f) turbulence amplitude profile. (a) - (c) are for low-collisionality phase, (d) - (f) are for high-collisionality phase. The peak positions of turbulence amplitude are indicated by dashed lines. T_e and n_e profiles are at $t = 4.517$ s in (a) and (b) and at $t = 6.517$ s in (d) and (e). Ionization rate is at $t = 4.334 - 4.564$ s in (b) and $t = 6.339 - 6.564$ s in (e). Turbulence is at $t = 4.5 - 4.7$ s in (c) and $t = 6.5 - 6.7$ s in (f).

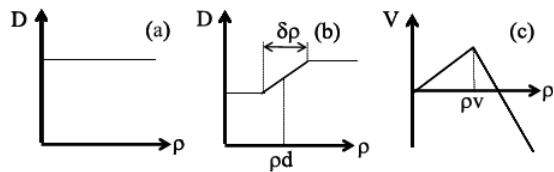


Fig. 7 Models for diffusion coefficient D and convection velocity V .

parameter diffusion coefficient model shown in Fig. 7 (b) was used; in that model, the diffusion coefficient was assumed to change at $\rho = \rho_d$ with a transition width $\delta\rho$. The convection velocity is assumed to be zero at the plasma center and to increase linearly and change slope at $\rho = \rho_v$. In this analysis, the transitions of D and V (ρ_d and ρ_v) were set to 0.7 and the transition width of D ($\delta\rho$) was set to 0.1. These choices reproduce the modulation amplitude, phase, and equilibrium profile.

The collisionality dependences of core ($\rho = 0.4 - 0.7$) and edge values ($\rho = 0.7 - 1.0$) of D and V are shown in Fig. 8. The normalization of collisionality was performed using the boundary between the $1/\nu$ and plateau regimes of neoclassical transport of a stellarator/helical device [5]. To compare D and V with and without RMP, several modulation experiments were conducted by scanning N-NB power around densities in the range of $1 - 3 \times 10^{19} \text{ m}^{-3}$. The analyzed D and V from the shot in Fig. 3 are indicated in Fig. 8 by the filled colored symbols. As shown in Fig. 8,

clear differences are not seen with and without RMP. This indicates that RMP does not affect particle transport in the low-collisionality ($\nu_h^* < 1$) phase. In all the data, core V is positive and outwardly directed, both with and without RMP. This indicates that the density profile is hollow in this data set.

Note that the profiles are almost identical in the low-collisionality phase with and without RMP, and that particle transport coefficients are also almost identical. As long as an island is healed, particle transport cannot be affected by an RMP field.

As described in Sec. 3.1, it is qualitatively clear that RMP can enhance particle transport in the high-collisionality phase. However, quantitative differences in particle transport with and without RMP remain unresolved for the high-collisionality phase. For quantitative analysis, the local particle confinement time was estimated and compared with and without RMP. Equation (1) can be rearranged to

$$\tau_p(\rho) = \frac{\int_0^\rho n_e d\rho}{\int_0^\rho S d\rho - \int_0^\rho \rho d n_e / dt}. \quad (4)$$

Here, $\tau_p(\rho)$ is the local particle confinement time at position ρ . Collisionality dependence of $\tau_p(\rho)$ is shown in Fig. 9. The figure shows that, in the low-collisionality phase, the spatially averaged τ_p in the core ($\rho = 0.4 - 0.7$) and in the edge ($\rho = 0.7 - 1.0$) region are almost same with and without RMP. This is consistent with the results in Fig. 8. The difference with and without RMP becomes ev-

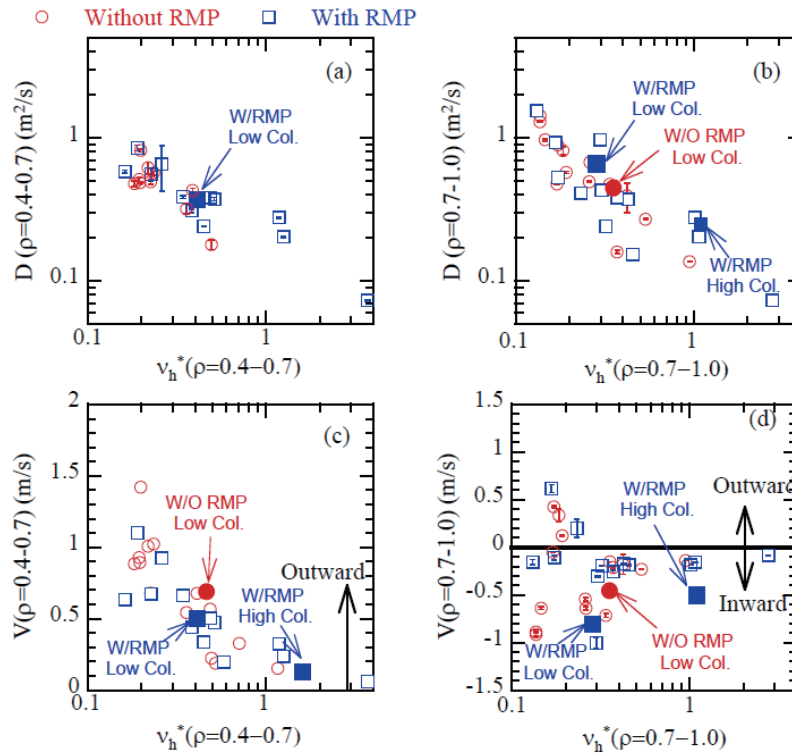


Fig. 8 Collisionality dependence of diffusion coefficients at (a) $\rho = 0.4-0.7$ and (b) $\rho = 0.7-1.0$, convection velocity (c) at $\rho = 0.4-0.7$ and (d) at $\rho = 0.7-1.0$. The data from Fig. 3 are indicated by the filled colored symbols.

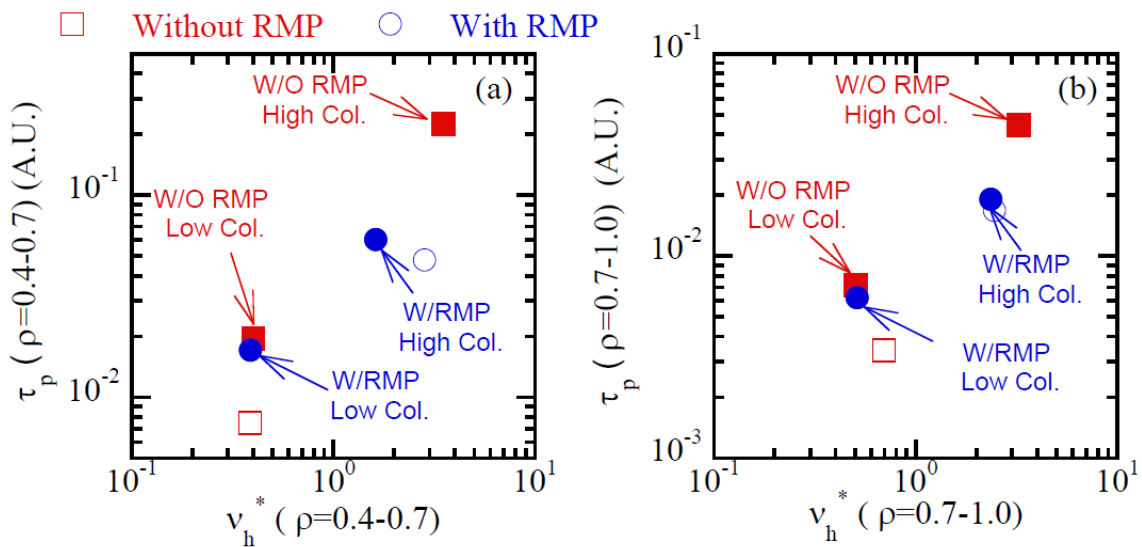


Fig. 9 Collisionality dependence of spatially averaged particle confinement time at (a) $\rho = 0.4-0.7$ and (b) $\rho = 0.7-1.0$. The data from Fig. 3 are indicated by the filled colored symbols.

ident at higher collisionality. The value of core τ_p without RMP in the high-collisionality phase of Fig. 3 (shot 105565 $t = 6.34-6.56$ s) is 3.7 times larger than the value in the high-collisionality phase of Fig. 3 with RMP (shot 105549, $t = 6.34-6.56$ s). This factor becomes 2.4 in the edge ($\rho = 0.7-1.0$) region. Although the present data set is limited, Fig. 9 suggests that particle transport is enhanced in the high-collisionality phase with RMP.

4. Discussion and Summary

The effects of $m/n = 1/1$ RMP on particle transport was investigated in LHD. The experiments were conducted in the outward shifted configuration, where $R_{ax} = 3.9$ m and the main plasma was surrounded by a thick ergodic layer.

In the low-collisionality phase ($v_h^* < 1$), almost no differences were observed with and without RMP. Spatial

profiles of n_e , T_e , and ion-scale turbulence were almost identical. There was no visible difference in D and V with and without RMP. Both $m/n = 2/1$ and $m/n = 1/1$ islands were healed.

In contrast, in the high-collisionality phase ($\nu_h^* > 1$), clear differences in particle transport characteristics were observed. With RMP, flattening of n_e and T_e occurred at around $\rho = 1.0$ because of the formation of an $m/n = 1/1$ island. With RMP, higher external fueling introduced lower densities compared to the case without RMP. This clearly shows that RMP enhances particle transport. Quantitatively, the local particle confinement time was higher by a factor of 3.7 in the core ($\rho = 0.4 - 0.7$) and 2.4 in the edge ($\rho = 0.7 - 1.0$) without RMP than with RMP. The collisionality dependence of τ_p suggests that the enhancement of particle transport with RMP increases with collisionality.

For more precise arguments, density modulation experiments are necessary in the high-collisionality regime. Larger modulation amplitudes or lower modulation frequencies will be necessary to modulate the density in the high-collisionality phase.

In the high-collisionality phase, turbulence profiles were different with and without RMP, although there was almost no difference in the low-collisionality phase. Further detailed investigation is necessary to understand the role of turbulence on RMP effects.

The results reported in this paper refer to the outward shifted configuration ($R_{ax} = 3.9$ m). At this configuration, mitigation of giant ELM has been reported and attributed to the enhancement of particle transport with RMP [13]. This indicates that, by enhancing particle transport, RMP can be used as a tool for controlling ELM mitigation.

Recent results about RMP effects at the inward shifted configuration, where $R_{ax} = 3.6$ m and better confinement

was achieved [14], also show enhancement of particle transport in the low-collisionality region ($\nu_h^* < 1$) [15]. Thus, the effects of RMP on particle transport depend on magnetic configuration as well as on collisionality effects. A systematic study of configuration effects is now in progress.

The enhancement of particle transport is similar to observations in tokamaks [16]. In LHD, the enhancement occurs only with the appearance of an island, while in tokamaks, flattening of n_e and T_e induced by RMP has not been reported. Investigation and comparison of the RMP impact on helical and tokamak plasmas will provide more detailed insight into the effects of RMP on particle transport.

- [1] T. Evans *et al.*, *Nature Physics* **2**, 419 (2006).
- [2] K. Toi *et al.*, proceeding of 23rd FEC 2010, October 11-16, Daejeon, Korea (2010).
- [3] Y. Suzuki *et al.*, *Nucl. Fusion* **46**, L19 (2006).
- [4] Y. Narushima *et al.*, *Nucl. Fusion* **48**, 075010 (2008).
- [5] K. Tanaka *et al.*, *Fusion Sci. Technol.* **58**, 70 (2010).
- [6] I. Yamada, K. Narihara, R. Yasuhara *et al.*, *Fusion Sci. Technol.* **58**, 345 (2010).
- [7] K. Tanaka, C. Michael, L.N. Vyacheslavov *et al.*, *Rev. Sci. Instrum.* **79**, 10E702 (2008).
- [8] Y. Narushima *et al.*, *Nucl. Fusion* **51**, 083030 (2011).
- [9] C.C. Hegna, *Phys. Plasmas* **19**, 056101 (2012).
- [10] M. Goto *et al.*, *Phys. Plasmas* **9**, 4316 (2002).
- [11] M. Goto *et al.*, *Nucl. Fusion* **51**, 023005 (2011).
- [12] K. Tanaka *et al.*, 24th FEC 2012, October 8-13, San Diego, USA (2012).
- [13] K. Toi *et al.*, 24th FEC 2012, October 8-13, San Diego, USA (2012).
- [14] H. Yamada *et al.*, *Nucl. Fusion* **45**, 1684 (2005).
- [15] M. Jakubowski *et al.*, *Nucl. Fusion* **53**, 113012 (2013).
- [16] S. Mordijck *et al.*, *Phys. Plasmas* **19**, 056503 (2012).